frontiers | Frontiers in Physics

TYPE Original Research
PUBLISHED 24 May 2024
DOI 10.3389/fphy.2024.1383835

OPEN ACCESS

EDITED BY
Hao Hu,
Nanjing University of Aeronautics and Astronautics, China

REVIEWED BY
Giuseppe Brunetti,
Politecnico di Bari, Italy
Juan-Feng Zhu,
Singapore University of Technology and Design, Singapore

*CORRESPONDENCE
Dongmei Liu,
dmliu@scnu.edu.cn
Min Gu,
mingu@m.scnu.edu.cn

†These authors have contributed equally to this work and share first authorship

RECEIVED 08 February 2024
ACCEPTED 10 May 2024
PUBLISHED 24 May 2024

CITATION
Sun C, Wang Q, Liang J, Wang W, Liu D, Chen Z and Gu M (2024), Theoretical realization of tunable hollow beams using a periodical ring structure with a complex phase.
Front. Phys. 12:1383835.
doi: 10.3389/fphy.2024.1383835

Theoretical realization of tunable hollow beams using a periodical ring structure with a complex phase

Changwei Sun[1†], Quansen Wang[1†], Jing Liang[1†], Wencong Wang[1], Dongmei Liu[1,2*], Zhenhua Chen[3] and Min Gu[1*]

[1]Guangdong Provincial Key Laboratory of Quantum Engineering and Quantum Materials, School of Physics, South China Normal University, Guangzhou, China, [2]Guangdong Provincial Engineering Research Center for Optoelectronic Instrument, School of Electronics and Information Engineering, South China Normal University, Foshan, China, [3]National Laboratory of Solid State Microstructures, College of Engineering and Applied Sciences, Nanjing University, Nanjing, China

Hollow beam is a peculiar structure beam, which has been widely used in various areas. Here, we propose a novel diffraction optical element to generate tunable hollow beams. This element is composed of periodic concentric rings. The phase of each ring is periodically distributed between $-\pi$ and π and satisfies a complex variable function. By tuning the parameters of the structure, we can flexibly manipulate the size and length of the hollow beam. The length of the beam can be increased from 98 λ to 248 λ, and the full width at half maximum varies from 0.43 λ to 0.61 λ. Moreover, the light intensity and side lobe of the hollow beam can also be regulated using the designed diffraction optical element. The potential applications of this highly tunable hollow beam include optical nanomanipulation, microscopic imaging, and nanolithography.

KEYWORDS

tunable hollow beams, complex phase, diffraction limit, azimuthally polarized wave, full width at half maximum

1 Introduction

Hollow beams have various applications in micro- and nano-processing [1], microscopic imaging [2, 3], photolithography [4], particle manipulation [5, 6], and optical wrenches [7, 8]. To date, several beam generation methods have been proposed, including modulating polarized beams to produce length-adjustable light needles or hollow beams [9], using a 4 π confocal system to backpropagate the radiation field to generate multisegment hollow beams [10], or creating a spatial optical tube of prescribed characteristics [11]. Chen et al. [12] produced a section of a hollow beam with uniform intensity by focusing a vortex beam through a phase-type spatial light modulator for the first time in 2018. Although these reported methods produce hollow beams with uniform light intensities, attributes such as the length and full width at half maximum (FWHM) of these hollow beams must be improved.

In recent years, a circular diffraction optical element (DOE) with a subwavelength structure has been applied to numerous applications such as super oscillating focusing [13–15], hollow dark rings [16–18], and optical needles [19–22]. Because of its ability to generate sub-diffractive beams, the circular DOE also provides a new solution for generating hollow beams with sub-diffractive properties. In a previous study, Wu et al. [16] designed a far-field diffractive planar lens based on a binary phase mask and used it

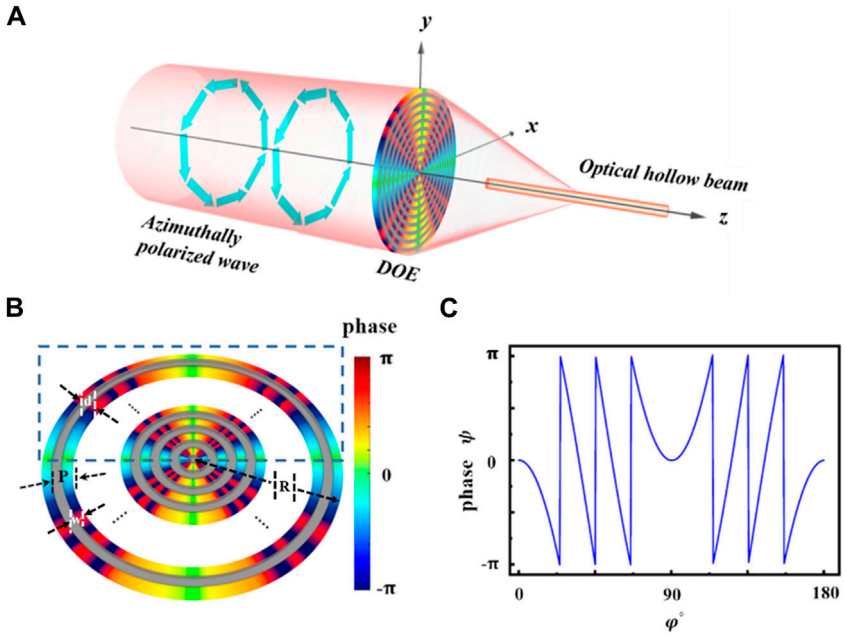

FIGURE 1
(A) Realization of the hollow beam by passing an angularly polarized light through the designed DOE. **(B)** Schematic of the DOE. The colored rings represent the transmitted region with a modulated phase, and the gray rings denote areas that are opaque. **(C)** Phase distribution for a half cycle when $m = 1$ and $n = 3$.

to produce a dark ring with an FWHM of 0.546 λ (where λ denotes wavelength), which beats the diffraction limit, at a focal length of 300 λ. Chen et al. [23] used a binary phase-type planar lens and experimentally produced a hollow beam with a length of 10 λ and a minimum FWHM of 0.34 λ for the first time. By using a DOE combined with spatial angular spectral compression, they further extended the length of the hollow beam to 100 λ and observed an optical hollow beam with subwavelength transverse dimensions within the nondiffractive propagation distance of 94 λ [24].

However, in most of the mentioned methods for designing DOE, which either involves subwavelength structure or is pure phase-type or pure amplitude-type. The generated the hollow beams cannot simultaneously achieve good FWHM and length. To obtain multiple hollow beams with different attributes, many sets of DOEs are required, and the structural parameters of each optimized DOE involve complex and time-intensive algorithms, which considerably limit the practical applicability of these components. In this study, we designed a novel DOE structure that does not require secondary optimization and produces a hollow beam with a sufficiently long length and narrow FWHM. The length, FWHM, intensity, and side lobe of the hollow beam can be tuned with minor adjustments of the designed structure. The length of the hollow beam can be adjusted from 98 λ (minimum limit) to 248 λ (maximum limit). The overall FWHM of the hollow beam can be adjusted from 0.43 λ (minimum limit) to 0.61 λ (maximum limit). The largest distance at which we can still observe the hollow beam is $z = 303\,\mu m$ (approximately 285 λ). Moreover, we can tune the intensity and side lobe of the hollow beam by varying the phase modulation factor.

2 Theory

Inspired by the cosine-phase grating [25], we designed a new DOE, composed of an annular structure and a complex phase, to realize a tunable hollow beam. As shown in Figure 1B, the designed DOE is composed of periodic concentric rings; the colored rings represent the regions with modulated phase, and the gray regions have zero transmittance and no phase modulation. The period P of these rings is equal to w plus d, where w is the width of each ring and d is the distance between two ring belts. The phase distribution in each modulated ring satisfies the function $(n, m) = 2\pi n \cos^2(m\varphi)$, where n and m are the modulation factors, and φ is the azimuthal angle. Because the phase does not change monotonically on the ring, we can call it a complex phase. Figure 1C shows the phase distribution for half a cycle when $n = 3$ and $m = 1$. Evidently, the phase does not vary monotonously along the angular direction; instead, it shows a cyclic variation varies between $-\pi$ and π. When an angular polarized beam illuminates the DOE, the resulting electric field can be described according to the Richards and Wolf vector diffraction theory as [26]

$$\boldsymbol{E} = \begin{bmatrix} e_x \\ e_y \\ e_z \end{bmatrix} = \frac{-iA}{\pi} \int_0^{\alpha} \int_0^{2\pi} \cos^{\frac{1}{2}}\theta \sin\theta \cos\varphi l(\theta) T(\theta, \varphi) \exp\left[ik\left(z\cos\theta + \rho\sin\theta\cos\varphi\right)\right] \begin{bmatrix} -\sin\varphi \\ \cos\varphi \\ 0 \end{bmatrix} d\varphi d\theta. \quad (1)$$

Here, A is a constant, θ is the angle between the focused beam and the optical axis, $\alpha = \arcsin\left(R/\sqrt{R^2 + z^2}\right)$, R is the radius of the structure, z is the focal length, and the function $l(\theta)$ represents the

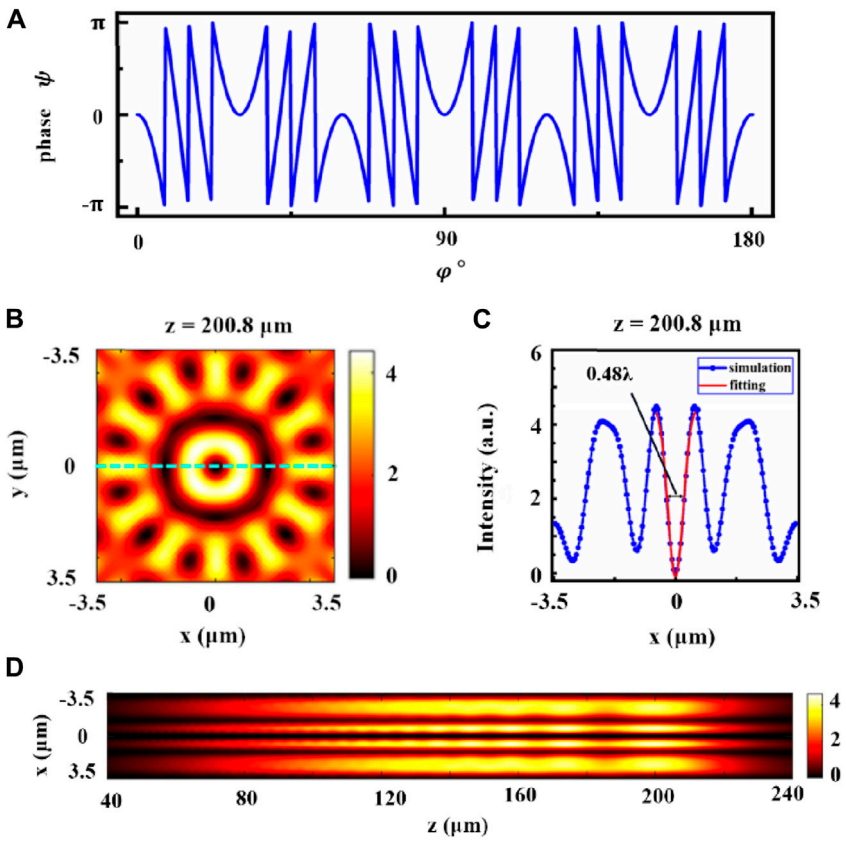

FIGURE 2
Hollow beam generated by the DOE with $P = 2.6\,\mu m$, $n = 3$, and $m = 3$. **(A)** Phase distribution for a half cycle when $m = 3$ and $n = 3$. **(B)** Intensity distribution of the hollow beam in the x-y plane at $z = 200.8\,\mu m$. **(C)** Intensity profile of the beam cross-section shown in **(B)**; the profile is fitted with an inverse Gaussian lineshape. **(D)** Propagation pattern of the hollow beam between $z = 40\,\mu m$ and $z = 240\,\mu m$.

amplitude distribution of the incident beam, which can be rewritten as:

$$l(\theta) = exp\left[-\left(\frac{sin\,\theta}{sin\,\alpha}\right)^2\right] J_1\left[2\frac{sin\,\theta}{sin\,\alpha}\right], \tag{2}$$

where $J_1[2\frac{\sin\theta}{\sin\alpha}]$ is a first order Bessel function of the first kind. And $T(\theta,\varphi) = t(\theta)\cdot t(\varphi)$ is the transmission function of the DOE. In this case, $t(\theta)$ is the amplitude distribution of DOE and can be expressed as:

$$t(\theta) = \begin{cases} 1 & \theta \in (\theta_{n-1}, \theta_n) \\ 0 & \theta \in (\theta_{n-2}, \theta_{n-1}) \end{cases}. \tag{3}$$

Further, $t(\varphi)$ is the phase distribution of DOE and can be expressed as:

$$t(\varphi) = \sum_{n=1}^{N} exp[i\psi(n,m)], \tag{4}$$

where N is the cumulative coefficient and the maximum value of n. In theory, we can take values of N from 1 to infinity. Considering the manufacturing technique of DOE, we chose N = 3 in the simulation. Thus, $t(\varphi) = exp[i\psi(1,m)] + exp[i\psi(2,m)] + exp[i\psi(3,m)]$. In the cylindrical coordinate system, e_x and e_y in Eq. 1 can be converted to:

$$e_\varphi = e_y\,cos\,\varphi - e_x\,sin\,\varphi, \tag{5}$$

$$e_\rho = e_x\,cos\,\varphi + e_y\,sin\,\varphi. \tag{6}$$

For an angularly polarized light, $e_\rho = 0$ and $e_z = 0$, which implies that only the angular component of the optical field needs to be considered in Eq. 1. Combined Eqs 2–6 and substituded into Eq. 1, the total field is obtained as:

$$E = \frac{-iA}{\pi}\sum_{n=1}^{N}\int_{\theta_{k-1}}^{\theta_k}\int_0^{2\pi} cos^{\frac{1}{2}}\theta\,sin\,\theta\,cos\,\varphi l(\theta)$$
$$exp[ik(zcos\theta + \rho\,sin\,\theta\,cos\,\varphi + 2\pi n\,cos^2(m\varphi))]d\varphi d\theta. \tag{7}$$

3 Simulation results and discussion

In this study, the genetic algorithm was employed to optimize the DOE for realizing a sub-diffraction hollow beam with an excellent performance. In the simulation, we choose titanium dioxide as the material for the phase modulation region of the DOE and silicon as the material for the opaque region, respectively. For the optimization process, we assume the modulation factors of phase distribution to be $n = 3$ and $m = 3$, and the number of concentric rings is considered to be 40. The reason we chose 40 is that the simulation results have similar phenomena when the number of rings is other numbers, such as

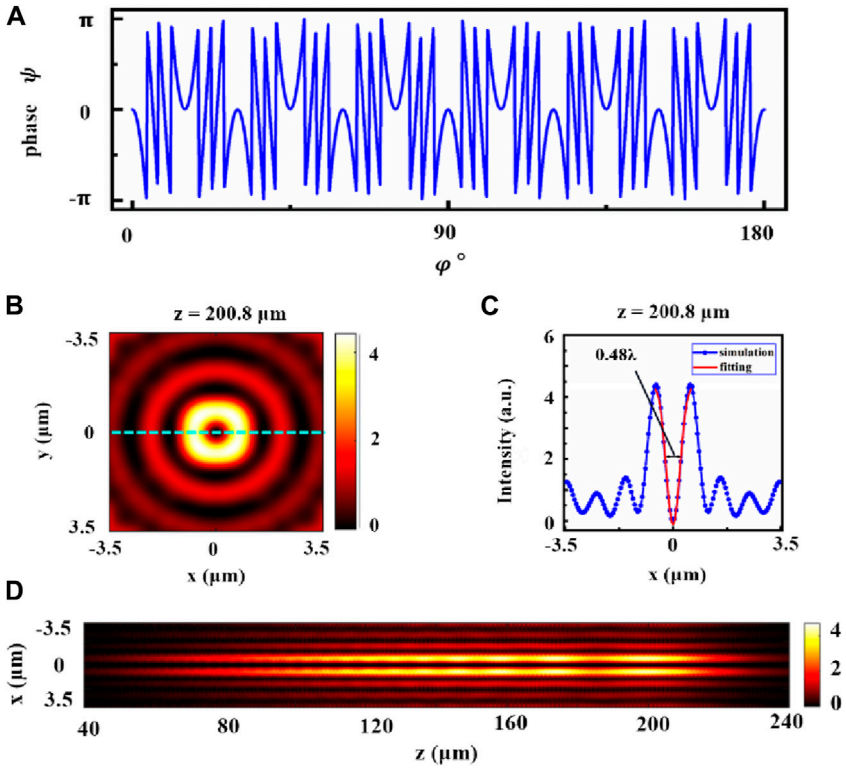

FIGURE 3
Hollow beam generated by the DOE with $P = 2.6\,\mu m$, $n = 3$, and $m = 6$. **(A)** Phase distribution for a half cycle when $m = 6$ and $n = 3$. **(B)** Intensity distribution of the hollow beam in the x-y plane at $z = 200.8\,\mu m$. **(C)** Intensity profile of the beam cross-section shown in **(B)**; the profile is fitted with an inverse Gaussian lineshape. **(D)** Propagation pattern of the hollow beam between $z = 40\,\mu m$ and $z = 240\,\mu m$.

35, 45, and 50, so here we take the structure with a ring number of 40 as an example. The width of these concentric rings, i.e., w and d of this DOE needs to be optimized, and the size and propagation length of the generated hollow beam are adopted as the objective functions for the genetic simulation. An angularly polarized light of wavelength 1.064 μm is assumed to be incident on the DOE. Following the optimization, the width of each ring is obtained as 1.3 μm ($w = d = 1.3\,\mu m$, $P = 2.6\,\mu m$), the radius R of the DOE is 104 μm. Under these considerations, Figure 2 shows the simulated performance of the hollow beams in terms of Eq. 7. For Figure 2D, three hollow beams are observed, one of which originates from the central light intensity distribution and the other two result from the side lobe effect. As shown in Figure 2A, it can be seen that when m increases from 1 to 3, the number of repeated changes of this complex phase within 0–180° also becomes three times. The central hollow beam exhibits an FWHM of 0.51 μm (see Figures 2C,D), i.e., 0.48 λ, which breaks the diffraction limit 0.5 λ. The simulations show that $z = 240\,\mu m$ is the largest distance at which a hollow beam is still observed, implying that the hollow beam obtained from such a DOE can be 140 λ long (Figure 2D). We also analyzed the side-lobe distribution around the hollow beam shown in Fig, 2. For instance, at $z = 200.8\,\mu m$, the beam intensity on the side lobe exhibits a flower structure with alternate bright and dark regions (petals), which represent the energy distributions (see Figure 2B).

However, the high-energy side lobe is almost adjacent to the hollow beam, and thus, severely restricts its applicability in different fields. To overcome this shortcoming, the energy on the side lobe of the hollow beam needs to be minimized.

Since the role of n is to adjust the overall light intensity of the hollow beam, and the light field intensity when $n = 3$ can already show the simulation results well, we fix the value of n unchanged. To restrain the high-energy side lobe, as indicated in Figure 3, we changed the modulation factor m of the complex phase in the simulation, while keeping the other parameters same as those shown in Figure 2. At $m = 6$, the FWHM and propagation length of the hollow beam are the same as before; however, the energy of the side lobe is reduced to only one-third of the main central-peak energy (see Figure 3B).

This is due to the fact that when m increases to 6, the number of complex phase changes also increases from 3 to 6, and this drastic phase change causes a redistribution of light field energy, so that the high-energy side lobe is pushed away from the central light field [28]. Evidently, a high-energy side lobe region coexists with the subwavelength features. In contrast, the low-energy side lobe is usually accompanied by large structural features. The uniquely designed DOE enabled a remarkable reduction in side-lobe energy while still retaining the subwavelength character.

Furthermore, we examined the dependence of the length and FWHM of the hollow beam on the DOE period. Considering the manufacturing technology as well as the subwavelength structure, we choose the period P of the DOE from 2.2 μm to 3.1 μm. As shown by the red curve in Figure 4A, the number of rings was assumed to be the same as before, and it was observed that the length of the generated hollow beam changed from 98λ to 248λ when the period P was varied from 2.2 μm to 3.1 μm, respectively. The FWHM of the hollow beam also changed as shown in Figure 4A, which indicates

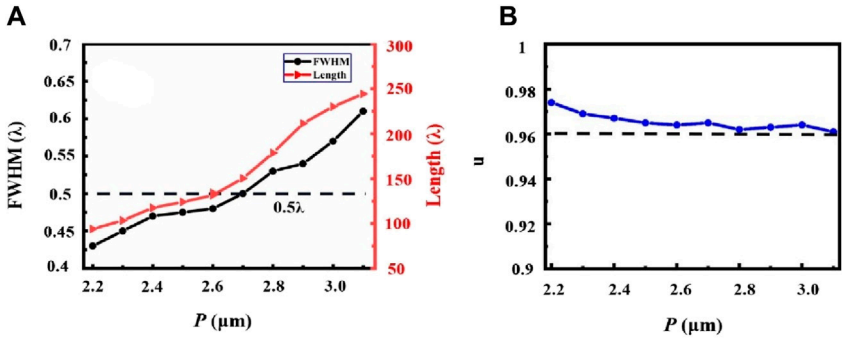

FIGURE 4
(A) Relationship between FWHM and Length of the hollow beam and the DOE period *P*. **(B)** Uniformity (*u*) of a hollow beam generated by DOE with different periods *P*.

that as the period increases, the FWHM of the generated hollow beam increases from 0.43 λ to 0.61 λ (the red solid line in Figure 4A). When $P > 2.7\,\mu m$, the resulting hollow-beam sizes surpass the diffraction limit (0.5 λ). To characterize the generated hollow beam, we define a uniformity function [27] as:

$$u = 1 - \frac{FWHM_{max} - FWHM_{min}}{FWHM_{max} + FWHM_{min}}, \tag{8}$$

where FWHM $_{max}$ and FWHM $_{min}$ are the maximum and minimum sizes of the generated hollow beam along the propagation distance.

As indicated in Figure 4B, the uniformity of the hollow beams is greater than 96% when P is between 2.2 and 3.1 μm. Notably, a smaller period results in a better uniformity of the hollow beam, because a DOE with a small period only generates a short hollow beam, which is characterized by a weak diffraction of light. Thus, it is easy to preserve the uniformity of the hollow beam generated by a DOE with a small period.

The aforementioned results indicate that a customizable hollow beam can be generated using the proposed DOE, which features a periodical annular structure. Each ring in this DOE structure has a complex phase, which is determined by the modulation factors n and m. The parameters such as the period and modulation factor of this DOE can be tuned to manipulate the size, length, and side lobe of the generated hollow beams. Moreover, multichannel hollow beams can also be obtained as evidenced in the simulations. Such flexibly tunable hollow beams have potential applications in diverse fields, because they act as optical potential wells that can trap high-refractive-index particles in regions with strong intensities as well as restrict low-refractive-index particles along their length. Thus, tunable hollow beams produced by the proposed DOE may offer new avenues for realizing optical micro- and nano-manipulation of particles.

4 Conclusion

In summary, we theoretically proposed a novel DOE for generating highly tunable hollow beams. The DOE consists of concentric rings with a phase that varies non-monotonically in the angular direction. By tuning the parameters of the DOE, such as its period, the size and propagation length of the generated hollow beam can be regulated from 0.43 λ to 0.61 λ and from 98 λ to 248 λ, respectively. In addition, the light intensity and side lobe of the hollow beam can also be controlled by changing the modulation factors. The extension of the current method to hollow beam may improve the transport ability down to nanometer scale, which would be very useful for manipulating nanoparticles with low refractive index along the beam. Moreover, such adjustable and flexible hollow beams have numerous promising applications, such as in practical nanofabrication, super-resolution microscopy, and nanolithography.

In the future, we will explore methods to extend the length of a hollow beam to the millimeter scale while keeping the transverse FWHM below the diffraction limit. Additionally, we will investigate how to generate a localized hollow beam array with transverse and longitudinal FWHMs below the diffraction limit while maintaining uniform light intensity.

Data availability statement

The raw data supporting the conclusion of this article will be made available by the authors, without undue reservation.

Author contributions

CS: Conceptualization, Data curation, Formal Analysis, Investigation, Methodology, Project administration, Software, Supervision, Validation, Visualization, Writing–original draft, Writing–review and editing. QW: Conceptualization, Data curation, Formal Analysis, Investigation, Methodology, Project administration, Software, Supervision, Validation, Visualization, Writing–original draft, Writing–review and editing. JL: Conceptualization, Data curation, Formal Analysis, Investigation, Software, Visualization, Writing–original draft, Writing–review and editing. WW: Data curation, Formal Analysis, Software, Supervision, Writing–original draft, Writing–review and editing. DL: Funding acquisition, Investigation, Supervision, Validation, Writing–original draft, Writing–review and editing. ZC: Data curation, Formal Analysis, Supervision, Validation, Writing–original draft, Writing–review and editing. MG: Conceptualization, Data curation, Formal Analysis, Funding

acquisition, Investigation, Methodology, Project administration, Software, Supervision, Validation, Visualization, Writing–original draft, Writing–review and editing.

Funding

The author(s) declare financial support was received for the research, authorship, and/or publication of this article. This study was supported by the National Natural Science Foundation of China (Grant No. 62375089), Guangdong Basic and Applied Basic Research Foundation (Grant No. 2022A1515140139), the Innovation Program for Quantum Science and Technology (Grant No. 2021ZD0303401) and Quantum Science Strategic Project of Guangdong Province (Grant No. GDZX2306004).

Conflict of interest

The authors declare that the research was conducted in the absence of any commercial or financial relationships that could be construed as a potential conflict of interest.

Publisher's note

References

1. Duocastella M, Arnold CB. Bessel and annular beams for materials processing. *Laser Photon Rev* (2012) 6(5):607–21. doi:10.1002/lpor.201100031

2. Weber N, Spether D, Seifert A, Zappe H. Highly compact imaging using Bessel beams generated by ultraminiaturized multi-micro-axicon systems. *JOSA A* (2012) 29(5):808–16. doi:10.1364/josaa.29.000808

3. Rogers ET, Zheludev NI. Optical super-oscillations: sub-wavelength light focusing and super-resolution imaging. *J Opt* (2013) 15(9):094008. doi:10.1088/2040-8978/15/9/094008

4. Gan Z, Cao Y, Evans RA, Gu M. Three-dimensional deep sub-diffraction optical beam lithography with 9 Nm feature size. *Nat Commun* (2013) 4(1):2061. doi:10.1038/ncomms3061

5. Peng F, Yao B, Yan S, Zhao W, Lei M. Trapping of low-refractive-index particles with azimuthally polarized beam. *JOSA B* (2009) 26(12):2242–7. doi:10.1364/josab.26.002242

6. Glushko B, Kryzhanovsky B, Sarkisyan D. Self-phase-matching mechanism for efficient harmonic generation processes in a ring pump beam geometry. *Phys Rev Lett* (1993) 71(2):243–6. doi:10.1103/physrevlett.71.243

7. Padgett M, Allen L. The angular momentum of light: optical spanners and the rotational frequency shift. *Opt Quan Electron* (1999) 31:1–12. doi:10.1023/a:1006911428303

8. La PA, Wang MD. Optical torque wrench: angular trapping, rotation, and torque detection of quartz microparticles. *Phys Rev Lett* (2004) 92(19):190801. doi:10.1103/physrevlett.92.190801

9. Liu T, Tan J, Liu J, Lin J. Creation of subwavelength light needle, equidistant multi-focus, and uniform light tunnel. *J Mod Opt* (2013) 60(5):378–81. doi:10.1080/09500340.2013.778343

10. Yu Y, Huang H, Zhou M, Zhan Q. Engineering of multi-segmented light tunnel and flattop focus with designed axial lengths and gaps. *Opt Commun* (2018) 407:398–401. doi:10.1016/j.optcom.2017.09.075

11. Zeng Y, Chen M, Lin S, Huang H, Wu P, Zhou M, et al. Creating a spatial optical tube of prescribed characteristics. *Opt Commun* (2022) 506:127581. doi:10.1016/j.optcom.2021.127581

12. Chen J, Xu Q. Superlong uniform light tunnel created by focusing radially polarized vortex beam. *J Appl Phys* (2018) 124(4). doi:10.1063/1.5033926

13. Qin F, Huang K, Wu J, Teng J, Qiu CW, Hong M. A supercritical lens optical label-free microscopy: sub-diffraction resolution and ultra-long working distance. *Adv Mater* (2017) 29(8):1602721. doi:10.1002/adma.201602721

14. Zhu X, Fang W, Lei J, Li Z, Xie F, Cao Y, et al. Supercritical lens array in a centimeter scale patterned with maskless UV lithography. *Opt Lett* (2020) 45(7):1798–801. doi:10.1364/ol.389702

15. Rogers ET, Lindberg J, Roy T, Savo S, Chad JE, Dennis MR, et al. A super-oscillatory lens optical microscope for subwavelength imaging. *Nat Mater* (2012) 11(5):432–5. doi:10.1038/nmat3280

16. Wu Z, Jin Q, Zhang S, Zhang K, Wang L, Dai L, et al. Generating a three-dimensional hollow spot with sub-diffraction transverse size by a focused cylindrical vector wave. *Opt Express* (2018) 26(7):7866–75. doi:10.1364/oe.26.007866

17. Chen G, Wu Z-X, Yu A-P, Zhang Z-H, Wen Z-Q, Zhang K, et al. Generation of a sub-diffraction hollow ring by shaping an azimuthally polarized wave. *Scientific Rep* (2016) 6(1):37776. doi:10.1038/srep37776

18. Huang K, Shi P, Cao G, Li K, Zhang X, Li Y. Vector-vortex bessel–gauss beams and their tightly focusing properties. *Opt Lett* (2011) 36(6):888–90. doi:10.1364/ol.36.000888

19. Wang H, Shi L, Lukyanchuk B, Sheppard C, Chong CT. Creation of a needle of longitudinally polarized light in vacuum using binary Optics. *Nat Photon* (2008) 2(8):501–5. doi:10.1038/nphoton.2008.127

20. He J, Zhuang J, Ding L, Huang K. Optimization-free customization of optical tightly focused fields: uniform needles and hotspot chains. *Appl Opt* (2021) 60(11):3081–7. doi:10.1364/ao.418415

21. Wang S, Li X, Zhou J, Gu M. Ultralong pure longitudinal magnetization needle induced by annular vortex binary Optics. *Opt Lett* (2014) 39(17):5022–5. doi:10.1364/ol.39.005022

22. Diao J, Yuan W, Yu Y, Zhu Y, Wu Y. Controllable Design of super-oscillatory planar lenses for sub-diffraction-limit optical needles. *Opt Express* (2016) 24(3):1924–33. doi:10.1364/oe.24.001924

23. Chen G, Wu Z, Yu A, Zhang K, Wu J, Dai L, et al. Planar binary-phase lens for super-oscillatory optical hollow needles. *Scientific Rep* (2017) 7(1):4697. doi:10.1038/s41598-017-05060-2

24. Zhang S, Chen H, Wu Z, Zhang K, Li Y, Chen G, et al. Synthesis of sub-diffraction quasi-non-diffracting beams by angular spectrum compression. *Opt Express* (2017) 25(22):27104–18. doi:10.1364/oe.25.027104

25. Amidror I. The fourier-spectrum of circular sine and cosine gratings with arbitrary radial phases. *Opt Commun* (1998) 149(1-3):127–34. doi:10.1016/s0030-4018(98)80006-0

26. Huang K, Ye H, Teng J, Yeo SP, Luk'yanchuk B, Qiu CW. Optimization-free superoscillatory lens using phase and amplitude masks. *Laser Photon Rev* (2014) 8(1):152–7. doi:10.1002/lpor.201300123

27. Lin H, Jia B, Gu M. Dynamic generation of debye diffraction-limited multifocal arrays for direct laser printing nanofabrication. *Opt Lett* (2011) 36(3):406–8. doi:10.1364/ol.36.000406